Progress in Nuclear Energy 111 (2019) 97–108

Contents lists available at ScienceDirect

Progress in Nuclear Energy

journal homepage: www.elsevier.com/locate/pnucene

Evaluation of the criticality and reaction rate benchmark experiments utilizing UO_2F_2 aqueous solution of intermediate enrichment in spherical geometry at ORNL

Tanja Goričanec[a,b], Bor Kos[a,b], Gašper Žerovnik[a,1], Margaret A. Marshall[c], Ivan A. Kodeli[a], Igor Lengar[a], Žiga Štancar[a,b], John D. Bess[c], David P. Heinrichs[d], Soon S. Kim[d], Michael L. Zerkle[e], Luka Snoj[a,b,*]

[a] Jožef Stefan Institute, Jamova cesta 39, SI-1000, Ljubljana, Slovenia
[b] Faculty of Mathematics and Physics, University of Ljubljana, Jadranska ulica 19, SI-1000, Ljubljana, Slovenia
[c] Idaho National Laboratory, 1955 N. Fremont Ave., Idaho Falls, ID, 83415, USA
[d] Lawrence Livermore National Laboratory, 7000 East Avenue, Livermore, CA 94550, USA
[e] Bettis Atomic Power Laboratory, PO Box 79, West Mifflin, PA, 15122, USA

ARTICLE INFO

Keywords:
Benchmark experiment
Spherical geometry
UO_2
F_2
ICSBEP
IRPHEP
MCNP

ABSTRACT

An evaluation of the criticality and relative fission rate radial distribution experiments in an 69.2-cm diameter aluminium sphere filled with intermediately enriched UO_2F_2 aqueous solution is presented. An evaluation of the total experimental uncertainty has been performed within the framework of the International Criticality Benchmark Evaluation Project (ICSBEP) and International Reactor Physics Benchmark Evaluation Project (IRPhEP). In addition, the uncertainty due to the uncertainties in the nuclear data is evaluated in this paper. It has been determined that the highest contribution to the overall uncertainty in the effective multiplication factor k_{eff} is due to the uncertainty in the uranium enrichment (~550 pcm in k_{eff} due to the 4% uncertainty in ^{235}U enrichment). The highest experimental uncertainties in the relative fission rate profile in terms of the relative standard uncertainty (*Lrs*) are 0.032, 0.016, and 0.020 due to the uncertainty in guide tube diameter, filling tubes position, and detector position, respectively. It is estimated that the uncertainty in the nuclear data contributes approximately **400 pcm–1200 pcm** to the uncertainty in k_{eff} depending on the covariance data library used. k_{eff} and radial fission rates have been calculated with MCNP and COG Monte Carlo neutron transport codes and have been compared to the experimental benchmark values. In general, the various Monte Carlo codes have given similar results with deviations within uncertainties.

1. Introduction

Thousands of experiments in different reactors and fissile systems have been performed since 1940. Considerable knowledge, experience, equipment and financial resources were needed to execute these experiments. Their results are of great importance for nuclear technology, because they are a reference for the validation of the modern computer codes and nuclear data. To preserve this data, the Nuclear Energy Agency within the Organisation for Economic Co-Operation and Development (OECD/NEA) launched several projects aiming to collect, preserve and disseminate benchmark data. The aim of the International Criticality Safety Benchmark Evaluation Project (ICSBEP, 2016) is to collect the information of all criticality experiments (Briggs and Bess, 2011; Briggs et al., 2014; Dean, 2003), while the International Reactor Physics Experiment Evaluation Project (IRPhEP, 2017) is evaluating various physical parameters from fissile experiments: reaction rate distribution, neutron flux distribution, neutron energy spectrum, reactivity coefficient measurements, etc. Their goal is to compile experimental benchmark data into standardized format that allows analysts to easily use data to validate computer tools and nuclear data. In the ICSBEP and IRPhEP evaluations great effort is put into the determination of experimental uncertainties and the effect of each

* Corresponding author. Jožef Stefan Institute, Jamova cesta 39, SI-1000, Ljubljana, Slovenia.
E-mail addresses: tanja.goricanec@ijs.si (T. Goričanec), bor.kos@ijs.si (B. Kos), gasper.zerovnik@ijs.si (G. Žerovnik), margaret.marshall@inl.gov (M.A. Marshall), ivan.kodeli@ijs.si (I.A. Kodeli), igor.lengar@ijs.si (I. Lengar), ziga.stancar@ijs.si (Ž. Štancar), john.bess@inl.gov (J.D. Bess), heinrichs1@llnl.gov (D.P. Heinrichs), kim53@llnl.gov (S.S. Kim), michael.zerkle@unnpp.gov (M.L. Zerkle), luka.snoj@ijs.si (L. Snoj).
[1] Currently at Institute for Reference Materials and Measurements, EC-JRC-IRMM, Retieseweg 111, B-2440 Geel, Belgium.

https://doi.org/10.1016/j.pnucene.2018.10.024
Received 15 June 2018; Received in revised form 17 September 2018; Accepted 29 October 2018

experimental uncertainty on the evaluated quantity (e.g. multiplication factor) is determined. The majority of experiments performed in the last decades have already been evaluated. However, many important historical experiments still need to be analysed. Only scarce information about some of those experiments is available and the major source of information are experimental logbooks (Magnuson, 1958), which were handwritten by the personnel who performed the experiments. Nevertheless their results are of great importance, because some unique configurations and nuclear materials were used.

In this paper a series of criticality and reaction rate experiments performed with intermediate enriched UO_2F_2 aqueous solution in spherical geometry at ORNL (Oak Ridge National Laboratory) (Callihan, 1975; Magnuson, 1973) is described and evaluated.

In the ICSBEP and IRPhEP evaluated experimental benchmarks, the focus is mainly on the evaluation of experimental uncertainties and developing the benchmark model. In this paper however we performed an evaluation of uncertainties due to nuclear data and test methods to evaluate uncertainty in k_{eff} due to temperature. Moreover the paper presents one of the few evaluated experimental benchmarks featuring integral (criticality) as well as differential (reaction rate profile) physical quantities where a complete analysis of all uncertainties (experimental and calculation) is performed. Additionally the simple geometry is easy to model with several deterministic and Monte Carlo codes and can be used for validation and inter-comparison of transport codes and of perturbation and random sampling based sensitivity/uncertainty methods.

Evaluation of the criticality experiment was published in the ICSBEP (2016) Handbook under the identifier IEU-SOL-THERM-005 (Kaiba et al., 2016), while the reaction rate distribution evaluation was published in the IRPhEP (2017) Handbook under the identifier ORCEF-FUND-EXP-001 (Goričanec et al., 2018). The purpose of this paper is to present and summarize major findings in these evaluations. In the evaluations published in both benchmark handbooks the focus is in the determination of the experimental and benchmark model uncertainties. However, to be able to accurately compare calculations with the experimental results the calculation uncertainty, i.e. statistical uncertainty due to the Monte Carlo method and uncertainty due to nuclear data need to be determined as well (Snoj and Kodeli, 2014). The uncertainty in nuclear data consist of the uncertainty in cross sections and uncertainties in physical parameters such as average fission neutron multiplicity ($\bar{\nu}$), etc. In this paper the research was complemented with the evaluation of the effect of the uncertainty in the nuclear data on the evaluated quantity and with the comparison of the results obtained through different Monte Carlo neutron transport codes, i.e. MCNP (Goorley et al., 2012) and COG (Buck and Lent, 2002). The uncertainty due to the uncertainties in the nuclear data was calculated with two different codes SUSD3D (Kodeli, 2001) and SANDY (Fiorito et al., 2016) and 4 different cross section covariance libraries (JEFF-3.3 (Plompen, 2017), JENDL-4.0 (Shibata et al., 2011), SCALE-6.0 (Rearden and Jessee, 2016) and ENDF/B-VII.1 (Chadwick et al., 2011)).

The experimental configuration is presented in Section 2. The evaluation of the critical and the reaction rate experiments are summarized in Sections 3 and 4 including descriptions of the experimental uncertainties supplemented with the calculation uncertainties. The benchmark model of the experiments is presented in Section 5. The calculation steps and results of the cross section sensitivity/uncertainty analysis are given in Section 6, which is followed by a discussion.

2. Experimental description

Several series of critical experiments involving aqueous uranyl fluoride (UO_2F_2) solutions were performed at ORNL between the years 1958 and 1960 (Callihan, 1975; Magnuson, 1973). These experiments were performed by D.W. Magnuson and his team (Magnuson, 1958) to determine the conditions under which aqueous solutions of intermediate enriched uranium (37 wt.% ^{235}U) can be made critical and to determine basic physical parameters. A series of critical experiments were performed in different geometries (spherical and cylindrical) and at different U concentrations and solution heights in cylindrical geometry. Within this paper only the evaluation of the spherical geometry is presented, which was an unreflected 69.2 cm diameter sphere. The sphere was fabricated using 0.32 cm thick aluminium and coated on the inside with a heresite to prevent corrosion (Magnuson, 1958; Gwin and Magnuson, 1960). A heresite coating was also used in other benchmark experiments and its description (chemical formula: $(C_6H_5OH)_{10}(FeO)$, density: 1.138 g/cm^3, thickness: 0.03 inch) was found in different benchmark evaluations in the ICSBEP Handbook (ICSBEP, 2016) (identifiers: HEU-SOL-THERM-013 (Pitts et al., 1996) and U233-SOL-THERM-005 (Elam, 2016)). Different measured vertical and horizontal diameters were recorded in the experimental logbook (Magnuson, 1958), which suggested that the sphere was in fact an ellipsoid and the volume inside the sphere was measured to be 173.55 l by filling it with water. Experiments with different solutions, i.e. $U(93.2\%)O_2(NO_3)_2$, were performed in the same sphere and are described in more detail in the experimental logbook (Magnuson, 1958). The experimental configuration is shown in Fig. 1. It can be observed that the experiment took place in a room, below the sphere is a platform with a hole inside. Only scarce information about the surrounding structure was available from the references and the majority of information was obtained from the HEU-SOL-THERM-013 (Pitts et al., 1996) evaluation in ICSBEP Handbook (ICSBEP, 2016). The information (i.e. dimensions) that was not found in any of the references were deduced from Fig. 1. Three neutron detectors covered with paraffin were positioned on the platform. Below the platform two storage mixing tanks (slab and cylindrical shape) can be observed. 5 cm diameter fill and vent tubes (Gwin and Magnuson, 1960) were attached at the top and bottom of the sphere. Sphere was positioned on three supporting legs and had 2 aluminium bands attached.

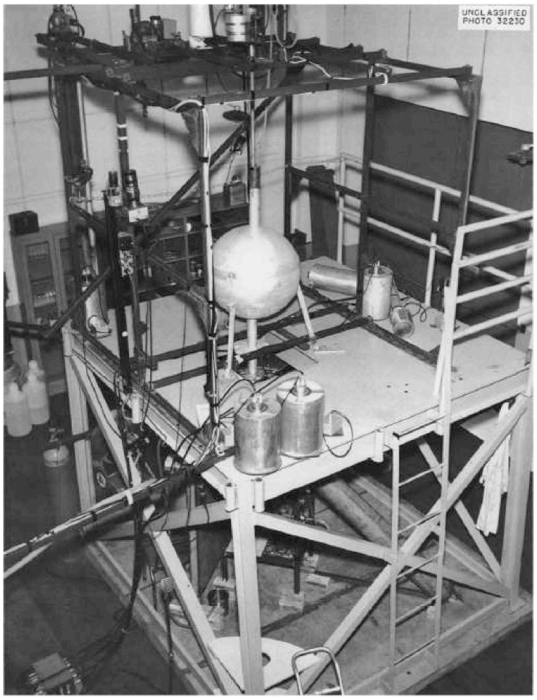

Fig. 1. View of experimental configuration (Gwin and Magnuson, 1960).

This paper summarizes the evaluation of the critical experiment performed in December 1958 with $U(37\%)O_2F_2$ and a uranium concentration of 49.15 mg uranium per g of solution. The full sphere was made critical by adjusting the chemical composition of uranium

solution through dilution (Magnuson, 1958). The height of the solution in the sphere was measured by a power driven probe, which closed the signal circuit when in contact with the liquid surface (Magnuson, 1958). The measured k_{eff} was 1.0005 (Magnuson, 1958) with no reported measurement uncertainty.

Measurements of the reaction rate radial profile were performed on December 12, 1958. The relative fission density was measured with two ^{235}U fission chambers located inside the sphere. The counters were suspended in the sphere through the upper tube. One of the fission chambers was moving through the sphere, while the other was at fixed position and served as the reference counter. Measurements were normalized first to the reference counter and then to the center of the sphere. The fission chambers had a 0.64 cm outer diameter and were 2.5 cm long (Callihan, 1975).

3. Evaluation of the experimental uncertainty of the critical experiment

The effects of the experimental and calculation uncertainties on the value of the multiplication factor were analysed using the MCNP 6.1 (Goorley et al., 2012) Monte Carlo neutron transport code and nuclear data from ENDF/B-VII.1 (Chadwick et al., 2011). A simplified model of the experiment, a bare spherical aluminium tank filled with solution, was used for evaluating the effect of the uncertainties. The simplified computational model used for the evaluation of the criticality experiment is presented in Fig. 2.

3.1. Evaluation of the effect of experimental uncertainties on reactivity

The available information describing experimental uncertainties is limited (e.g. ORNL reports (Gwin and Magnuson, 1960; Callihan, 1975), the experimental logbook (Magnuson, 1958) and other similar criticality benchmark experiments (Pitts et al., 1996; Marshall et al., 2010)). Some information is repeated stating different values (e.g. solution volume) or not given at all (e.g. surrounding structure). The effect of experimental uncertainties in different parameters on the value of the multiplication factor (k_{eff}) was evaluated. Uncertainties were determined by changing the corresponding parameter in the model for each uncertainty and calculating k_{eff} for each configuration. The change in multiplication factor due to the change in individual parameter (P_i), also called the sensitivity coefficient of k_{eff} to P_i, was obtained using Monte Carlo calculations and can be expressed as:

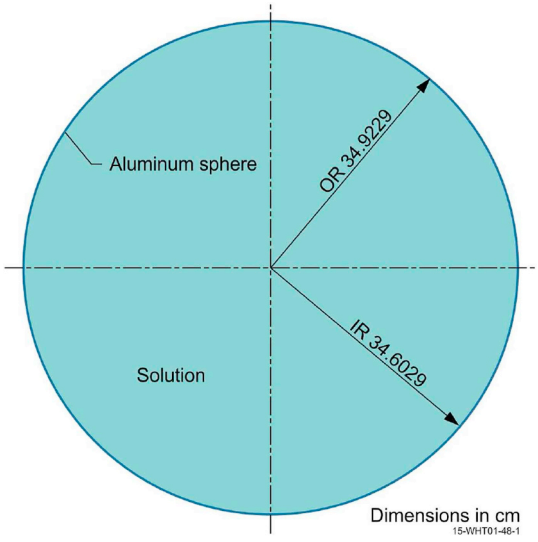

Fig. 2. Schematic view of the computational model for the criticality experiment.

Table 1
Evaluated experimental uncertainties for the criticality experiment.

Source of Uncertainty	1σ	Δk_{eff}
Volume	0.5%	0.0005
Solution density	$0.5\%/\sqrt{3}$	0.0010
Uranium concentration	$1.0\%/\sqrt{3}$	**0.0023**
Enrichment (^{235}U weight fraction)	4%/3	**0.0055**
^{234}U weight fraction	4%/3	Neg.
^{236}U weight fraction	4%/3	Neg.
Temperature (cross section)	$\Delta T = 6°C/\sqrt{12}$	0.0003
Al impurities concentration	Al Type 1100	Neg.
Al wall thickness	0.005 cm	Neg.
heresite thickness	0.0762 cm	0.0002
Solution impurities uncertainty	difference between 2 reports	**0.0023**
Departure from sphericity	0.0127 cm	Neg.
Combined experimental uncertainty		**0.0065**

$$\frac{\Delta k_{eff}}{\Delta P_i} = \frac{k_{P_1} - k_{ref}}{P_1 - P_{ref}}, \quad (1)$$

where indices ref and 1 represent reference and perturbed calculations, respectively. The 1σ experimental uncertainty (e.g. due to the scarce information) was evaluated for each parameter and is reported in the second column of Table 1. The uncertainty in the k_{eff} value (σ_{ki}) due to the experimental uncertainty in an individual parameter (σ_{Pi}) can be estimated as:

$$\sigma_{ki} = \frac{\Delta k_{eff}}{\Delta P_i}\sigma_{Pi}, \quad (2)$$

neglecting higher order sensitivity uncertainty coefficients. Uncertainty effects smaller than the Monte Carlo statistical uncertainty (± 0.0001 Δk) were considered negligible. The source and value of individual uncertainties is described in detail in the experiment evaluation in the ICSBEP (2016) Handbook. Evaluated 1σ experimental uncertainties and their effect on the k_{eff} value are summarized in Table 1. The total experimental uncertainty was obtained by taking the square root of the sum of the squares of the individual uncorrelated uncertainties:

$$\sigma_{tot} = \sqrt{\sum_{i=1}^{N} \sigma_{ki}^2}. \quad (3)$$

The total experimental uncertainty is reported in Table 1 to be σ_{tot} = 0.0065 Δk. The largest contribution is due to the uncertainty in the fuel enrichment.

3.1.1. Uncertainty due to temperature

Through the evaluation process it was determined that the multiplication factor is highly sensitive to the variations in solution temperature. Therefore the evaluation of the uncertainty in temperature is described in more detail. In the experimental logbook (Magnuson, 1958) the temperature was described to range between 293 K and 299 K. For analysing the effect of the temperature change on the k_{eff} value three different effects had to be taken into account: water density (Density), Doppler broadened cross sections (Doppler), and the thermal scattering kernel (S(α,β)). The effect of water density change was analysed during the solution density change evaluation and was not evaluated further. The contribution to the temperature coefficient of reactivity due to the water density change was estimated to be: $\frac{\Delta\rho}{\Delta T}$(Density) = (−8.08 ± 0.48) pcm/K. It is important to note that the volume expansion of the spherical tank is neglected. The technique of pseudo materials (Conlin et al., 2005) was used to evaluate the effect due to Doppler broadening of cross sections. The atomic density fractions at 299 K were calculated using pseudo-materials method. The calculation was performed using ENDF/B-VII.1 (Chadwick et al., 2011) neutron cross section libraries at 293.6 K and 600 K. The difference in multiplication factor between the two Doppler broadened cross sections was − 0.00011Δk. The contribution to the temperature coefficient of

reactivity due to the Doppler broadening was determined to be: $\frac{\Delta\rho}{\Delta T}$(Doppler) = (−2.04 ± 1.11) pcm/K.

Special care was put into analysing the temperature dependence of the thermal scattering kernel. Hydrogen bound in water (H-H_2O) thermal scattering kernels were evaluated in 5 K intervals using different techniques:

- Using the LEAPR module of the NJOY code (MacFarlane et al., 2012) to prepare application specific S(α,β) files.
- Using MAKXSF code (Brown, 2006) to interpolate pre-calculated ENDF/B-VII.0 thermal scattering libraries to a desired temperature.
- Mixing of S(α,β) data similar as in the pseudo materials technique.

For the first technique, an internal Bettis nuclear data processing code was used to prepare finer temperature resolution ENDF/B-VII.0 H-H_2O thermal scattering kernels for use in this analysis. LEAPR input models were prepared at 5 K temperature intervals between 283 K and 368 K by interpolating/extrapolating between the temperature dependent tabulated fundamental physical model parameters (vibrational density of states and weights for the hindered rotation, bending, stretching, and translational modes) for the ENDF/B-VII.0 H-H_2O evaluation. The finer temperature resolution S(α,β) thermal scattering law data was then generated using the LEAPR module of the NJOY code (MacFarlane et al., 2012). The effect of thermal scattering kernel temperature dependence on the k_{eff} was determined by performing multiple MCNP calculations using S(α,β) data evaluated at different temperatures while retaining all other Doppler broadened cross sections at 293 K. The results (black color in Fig. 3 for MCNP using LEAPR) were compared with KENO V.a (SCALE 6.1 (Rearden and Jessee, 2016) with ENDF/B-VII.0 Chadwick et al. (2006) data library) calculations (red color in Fig. 3). To evaluate the contribution of the thermal scattering kernel to the temperature coefficient of reactivity a linear fit was made using the results for temperatures between 288 K and 303 K. The contribution from the thermal scattering kernel due to the temperature change of 6 K was evaluated from the linear fit taking into account Eqs. (1)–(3). Associated change in k_{eff} was $-0.00090\Delta k$. The contribution to the temperature coefficient of reactivity due to the thermal scattering kernel was determined from the linear fit of the LEAPR results to be: $\frac{\Delta\rho}{\Delta T}(S(\alpha,\beta)) = (-14.28 \pm 0.10)$ pcm/K. Taking into account the contributions from both the Doppler broadening and thermal scattering kernel contributions, the overall effect on k_{eff} is $-0.00101\Delta k$ and the total temperature coefficient of reactivity due to the cross sections and water density change is:

$$\frac{\Delta\rho}{\Delta T} = (-24.4 \pm 1.7)\ \text{pcm/K}. \quad (4)$$

It can be concluded that this experiment was very sensitive to temperature change, especially due to the temperature dependence of thermal scattering kernel and can therefore be used as a reference for testing H-H_2O thermal scattering kernel. Hereinafter, it was also used to test two additional methods for temperature dependent thermal scattering kernels and the results obtained using different methods were compared and are presented in Fig. 3.

The MAKXSF code (Brown, 2006) is a utility program for processing cross section library files for the MCNP Monte Carlo code. It can be used to create nuclear datasets at new temperatures including 3 basic operations (Brown, 2006):

- Doppler broaden the resolved resonance data to a higher temperature.
- Interpolate any unresolved resonance probability tables to the new temperature.
- Interpolate S(α,β) thermal scattering kernel data to the new temperature.

The MAKXSF code can only interpolate S(α,β) data between two existing libraries and extrapolation cannot be performed. Therefore the temperature of interest is limited with the minimum and maximum temperature of the original libraries. Using MAKXSF code the ENDF/B-VII.0 (Chadwick et al., 2006) and JEFF 3.1 (Koning et al., 2006) S(α,β) thermal scattering kernel data were generated in 5 K intervals between 298 K and 358 K using nuclear data libraries at (293.6 K, 350 K and 400 K for ENDF/B-VII.0 and 293.6 K, 323.6 K and 373.6 K for JEFF 3.1). The results are presented in Fig. 3 (with blue color for ENDF/B-VII.0 and magenta color for JEFF 3.1).

The method of mixing S(α,β) nuclear data libraries is not well known approach among the MCNP users (Donnelley, 2010). It is similar to the pseudo-material method (Conlin et al., 2005), however this method cannot be applied directly for the S(α,β) cross sections, because only one H-H_2O thermal scattering kernel (at only one temperature) can be used in MCNP for the same material. The method of mixing S(α,β) data includes creation of duplicate nuclear data libraries and changing linking identifiers in the duplicate. The method is described in detail in Donnelley (2010). For this method thermal scattering kernels at the same temperature as neutron cross sections for the ^{1}H isotope are taken. The S(α,β) data in the ENDF/B-VII.1 nuclear data library are tabulated in 50 K intervals, therefore the cross sections for the ^{1}H isotope were generated in 50 K intervals using the MAKXSF code. The results are presented in Fig. 3 with green color. For the mixing calculations the ^{1}H isotope was treated with the pseudo-materials (Conlin et al., 2005) method therefore the reference calculation was also performed with the ^{1}H isotope treated with the pseudo-materials (Conlin et al., 2005) method and without mixing S(α,β) data and instead data generated with MAKXSF code were used (results presented with orange color in Fig. 3).

It can be concluded that the results agree well with each other and show linear temperature dependence of thermal scattering kernel with slight deviations between different nuclear data libraries and different calculation methods. The ENDF/B-VII.0 and JEFF 3.1 nuclear data libraries were also compared in Fig. 3, where the deviation up to ~100 pcm can be observed between the two libraries. Results show good agreement within the uncertainties between both Monte Carlo codes (MCNP and SCALE). Results obtained using the LEAPR module of the NJOY code and the results obtained with MAKXSF code agree well with each other and the deviations are <50 pcm. Mixing method results using the original ENDF/B-VII.0 nuclear data libraries are represented in light green in Fig. 3. Results obtained with the mixing method of S

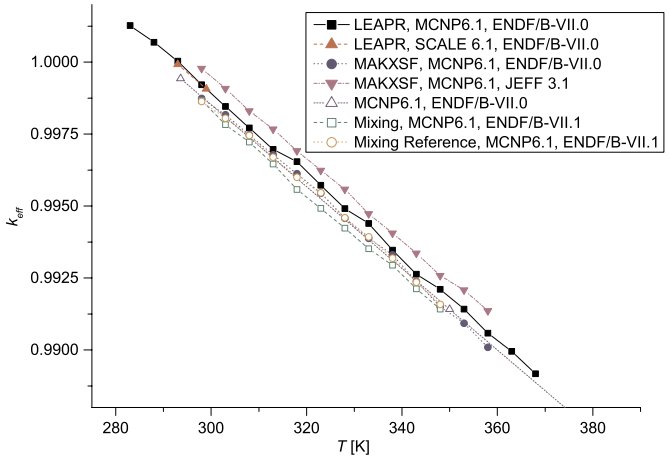

Fig. 3. Multiplication factor as a function of the temperature of the thermal scattering kernel using different techniques and nuclear data libraries. Standard deviation for all calculations is 0.00006 and was considered negligible and, for better visibility, not included in the graph.

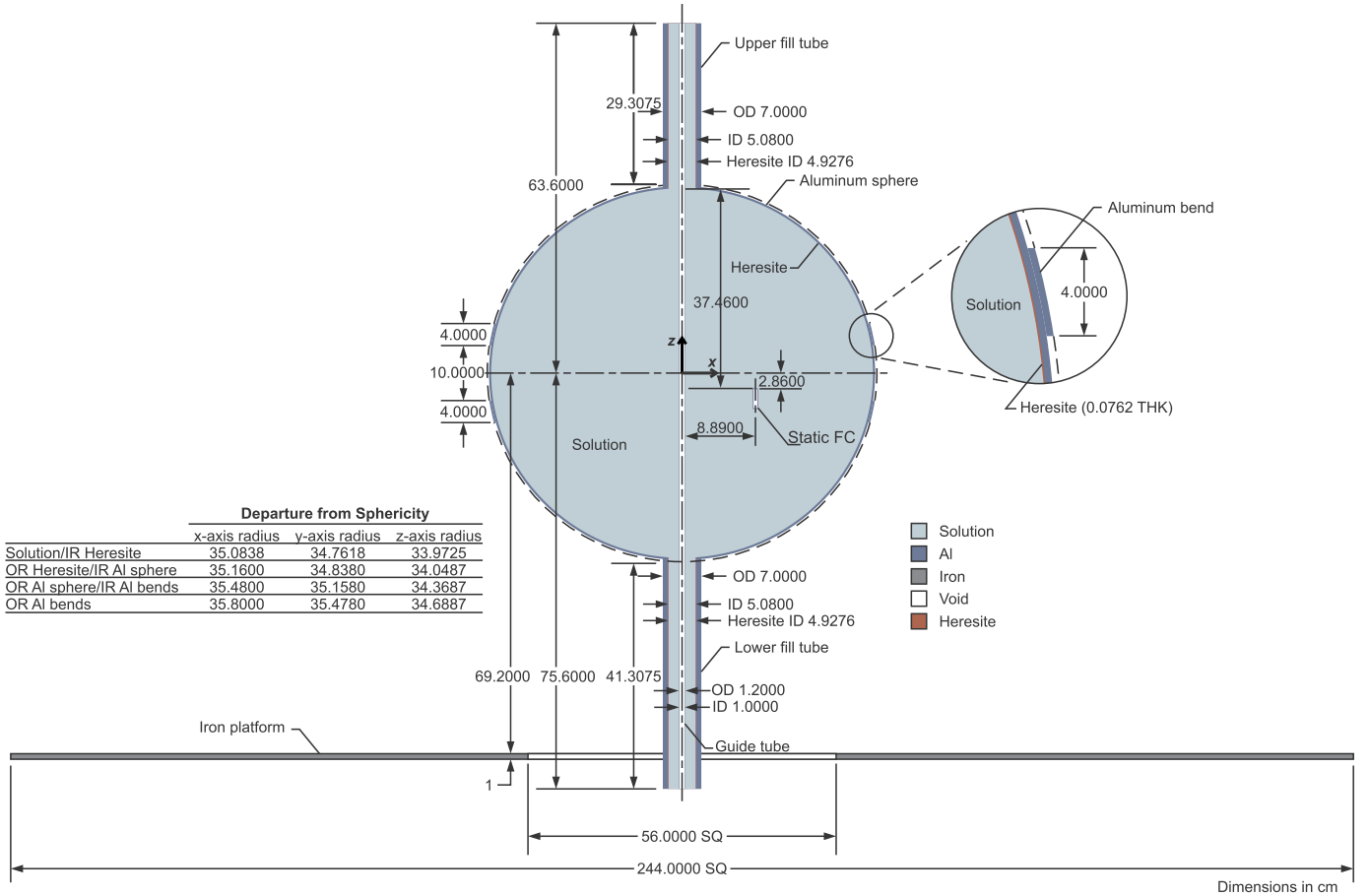

Fig. 4. Schematic view of the computational model for the reaction rate experiment.

(α,β) data are presented in green color in Fig. 3 and deviate from their reference calculation (presented in orange) with S(α,β) data generated with MAKXSF by <60 pcm.

4. Evaluation of the experimental uncertainty of reaction rate experiment

The experimental and calculation uncertainty for the reaction rate experiment were evaluated using the MCNP 6.1 (Goorley et al., 2012) Monte Carlo neutron transport code with ENDF/B-VII.1 (Chadwick et al., 2011) nuclear data libraries. When evaluating the reaction rate experiment it was assumed that the surrounding structure has a significant effect on the radial fission rate distribution. Therefore, some of the surrounding structures were included in the reference computational model: upper and lower filling tube, aluminium bands, heresite coating, moving rod, static counter and iron platform. The solution content was modelled as a flattened sphere instead of as a perfect sphere. The moving fission chamber was not modelled explicitly in the benchmark model and therefore its movement was not applied. Fig. 4 presents modelled geometry for the reaction rate calculations. Because the evaluation of experimental uncertainties was performed without explicit modelling of the moving counter, only a single calculation was sufficient to determine the response of all detector positions. Because in a single calculation the response of the static counter is constant, there was no need for an additional normalization to its response.

For evaluation of the experimental uncertainty, two new quantities were introduced for describing the behaviour of the calculated reaction rates during parameter variation. The first quantity, named the relative natural norm L_{nat}, represents the absolute value of maximum of L_i value, which is the relative difference in the fission reaction rate between the reference calculation $G_{r,i}$ and the calculation with a perturbed value of a specific parameter G_i in the i^{th} radial position:

$$L_{\mathrm{nat}} = \max(|L_i|) = \max\left(\left|\frac{G_i - G_{r,i}}{G_{r,i}}\right|\right), \tag{5}$$

where the index i goes over all measuring axial positions N. The second quantity is used as a measure for the relative standard uncertainty of the reaction rate calculations and can be expressed as:

$$L_{rs} = \sqrt{\frac{\sum_{i=1}^{N} L_i^2}{N}}. \tag{6}$$

When evaluating experimental uncertainties, different parameters were changed and results of the changed calculation were compared to the reference calculation. Different changes can affect the relative fission rate distribution differently. Most of them only have effect on the absolute value of the fission rate and do not change the relative radial profile of the fission rate, their impact is homogeneous through the entire sphere (e.g. enrichment, uranium concentration, solution density, etc.), while others can have different effect on the upper or lower part of the sphere or even only within one region of sphere. Therefore, great care must be taken to correctly analyse different effects. Due to the normalization to the position at the center of sphere and comparison to the reference calculation, the small initial MCNP standard deviation significantly increases and often deviations are within the uncertainty. During the evaluation of the deviations the L_i, L_{nat} and L_{rs} values were studied. It was determined that the L_{rs} value was optimal for describing variations through the entire radial profile and a negligible limit of $L_{\mathrm{rs}} < 0.001$ was applied. Uncertainties similar to those evaluated in the criticality experiment were analysed plus additional uncertainties due to detector position and the surrounding structures. Two different uncertainty effects are presented in Fig. 5, where we can

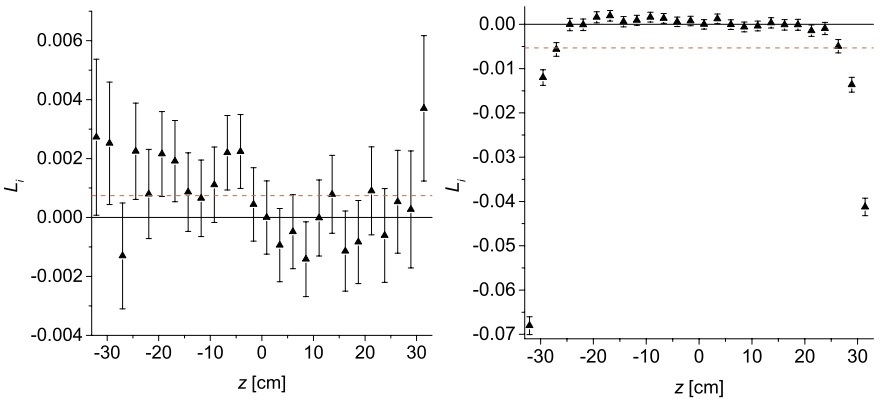

Fig. 5. Deviations in the relative fission rate represented with L_i values due to the -1σ uncertainty in uranium concentration (left) and due to the uncertainty (presence) in filling tubes (right) as a function of radial distance from the center of the sphere (radial positions in calculations are equal to the experimental positions of moving detector). Dashed red line represents the average value of L_i through the entire radial profile. article.)

Table 2
Evaluated L_{rs} values of individual uncertainties for the reaction rate experiment.

Source of Uncertainty	Average L_{rs}	Evaluating approach
Volume	0.003	All radial positions individually
Solution density	Negligible	Negligible
Uranium concentration	Negligible	Negligible
Enrichment (^{235}U weight fraction)	Negligible	Negligible
Departure from sphericity	0.006	All radial positions individually
Temperature (Doppler and Thermal)	Negligible	Negligible
Fissile deposit	0.004	Radial average
Aluminium bands	0.002	Radial average
Filling tubes	0.016	All radial positions individually
Filling tubes heresite thickness	Negligible	Negligible
heresite thickness	0.002	All radial positions individually
Iron platform	Negligible	Negligible
Al impurities	Negligible	Negligible
Al thickness	0.003	Radial average
Detector position	0.020	All radial positions individually
Solution impurities	0.002	Radial average
Surrounding structure	0.002	All radial positions individually
Guide tube diameter	0.032	All radial positions individually
Guide tube thickness	0.005	All radial positions individually
Guide tube heresite coating	0.002	Radial average
Static counter	0.002	Radial average
Measuring	0.0073	All radial positions individually
Total	0.043	

observe an approximately uniform effect of the uranium concentration change on the left graph. In comparison, the filling tubes were found to have a different effect in different radial positions, which is presented on the right graph in Fig. 5, where each radial position was treated individually. Uncertainty in the filling tubes was evaluated as half of the difference between results of calculation with and without them.

All of the evaluated average individual uncertainties are summarized in Table 2 in terms of L_{rs}. However, a different radial behaviour of these uncertainties must be considered and therefore the average total uncertainty is only used to assess the order of magnitude of the uncertainty. All the evaluated uncertainties were treated as uncorrelated and therefore they were summed in quadrature for establishing the total uncertainty. The calculated total uncertainty is averaged over the entire axial profile and is equal to: $L_{\mathbf{rs}} = 0.043$. Because of high deviations between the different radial positions the total uncertainty is not used in the further evaluation and the uncertainties are treated individually in each different radial position. Two significant contributions to the total uncertainty is the uncertainty in the guide tube diameter and the moving detector position. The total evaluated uncertainty for each measuring position was calculated by summing in quadrature the individual uncertainties above the negligible limit. The total evaluated uncertainties for each detector position are presented in Table 3, where the results are normalized values of the measured fission rate. It must be recognized that the reported uncertainties do not take into account the correlation between different radial positions. To assess the order of magnitude of the correlations between different measuring positions, the neutrons passing through the central position and contributing to the signal in other measuring positions were analysed. It was estimated that they contribute from ~1% up to ~12% to the overall signal in individual measuring position. It has to be noted that this is not a true measure of correlation, but only to evaluate the order of magnitude of contribution. In future research, correlations between different parameters from a single Monte Carlo calculation will be studied. However, this is out of the scope of this paper.

5. The benchmark model

The benchmark model of the criticality experiment is a simplified model, that was also used for the experimental uncertainty evaluation and is presented in Fig. 2. It consists of an perfect aluminium sphere with outside radius of 34.9229 cm and inside radius of 34.6029 cm.[2] It

[2] Values are specifications for the benchmark model and do not resemble actual accuracy of the data.

Table 3
Experimental results with evaluated relative experimental uncertainties in individual measuring position for the reaction rate experiment.

Detector position [cm]	Normalized relative fission rate
−32.1	0.128 (1 ± 0.141)
−29.6	0.233 (1 ± 0.062)
−27.0	0.316 (1 ± 0.037)
−24.5	0.411 (1 ± 0.030)
−22.0	0.507 (1 ± 0.019)
−19.4	0.597 (1 ± 0.021)
−16.9	0.689 (1 ± 0.016)
−14.3	0.770 (1 ± 0.012)
−11.8	0.835 (1 ± 0.011)
−9.3	0.901 (1 ± 0.011)
−6.7	0.946 (1 ± 0.011)
−4.2	0.977 (1 ± 0.010)
−1.6	0.998 (1 ± 0.010)
0.9	1.000 (1 ± 0.009)
3.5	0.984 (1 ± 0.010)
6.0	0.948 (1 ± 0.010)
8.5	0.917 (1 ± 0.009)
11.1	0.858 (1 ± 0.010)
13.6	0.787 (1 ± 0.011)
16.2	0.715 (1 ± 0.012)
18.7	0.624 (1 ± 0.016)
21.2	0.531 (1 ± 0.019)
23.8	0.435 (1 ± 0.025)
26.3	0.337 (1 ± 0.036)
28.9	0.230 (1 ± 0.056)
31.4	0.110 (1 ± 0.114)

was filled with UO_2F_2 solution with density of 1.057 g/cm^3 and uranium concentration of 49.13 mg/g. Solution impurities were not included.

The benchmark model for the fission rate radial distribution measurements was the simplified model used for the experimental uncertainty evaluation and is presented in Fig. 4. In contrast to the criticality experiment benchmark model, in the reaction rate benchmark model the departure from sphericity was taken into account, as well as filling tubes, moving tube, aluminium bands, heresite coating, iron platform and static fission chamber. Those details were added due to the high dependence of the radial fission rate distribution on the nearby structures and tank shape. Solution filling the spherical tank had the same characteristics as in the criticality benchmark model.

Calculations were performed using MCNP6.1 (Goorley et al., 2012) and ENDF/B-VII.1 (Chadwick et al., 2011) cross sections. Both benchmark models were simplified and some surrounding structure, solution impurities, etc. were not taken into account. This led to a bias between the benchmark model and experimental values. Biases were determined for both benchmark model values.

5.1. Evaluation of biases

In the simplified computational model of the criticality experiment the following structures were removed: air, aluminium impurities, heresite coating, surrounding structure (see Fig. 6), solution impurities and departures from sphericity. The statistical uncertainty in each individual Monte Carlo simulation used to estimate the bias contributions was ±0.00009 Δk. All evaluated biases are summarized in Table 4. The overall bias was calculated as the sum of the individual bias contributions. The total simplification bias uncertainty is calculated as sum of squares of individual contributions. A negligible limit of 0.0001 was used and biases smaller than the negligible limit were not included in the overall bias calculation, however the statistical uncertainty of the bias calculation was preserved for the calculation of overall bias uncertainty.

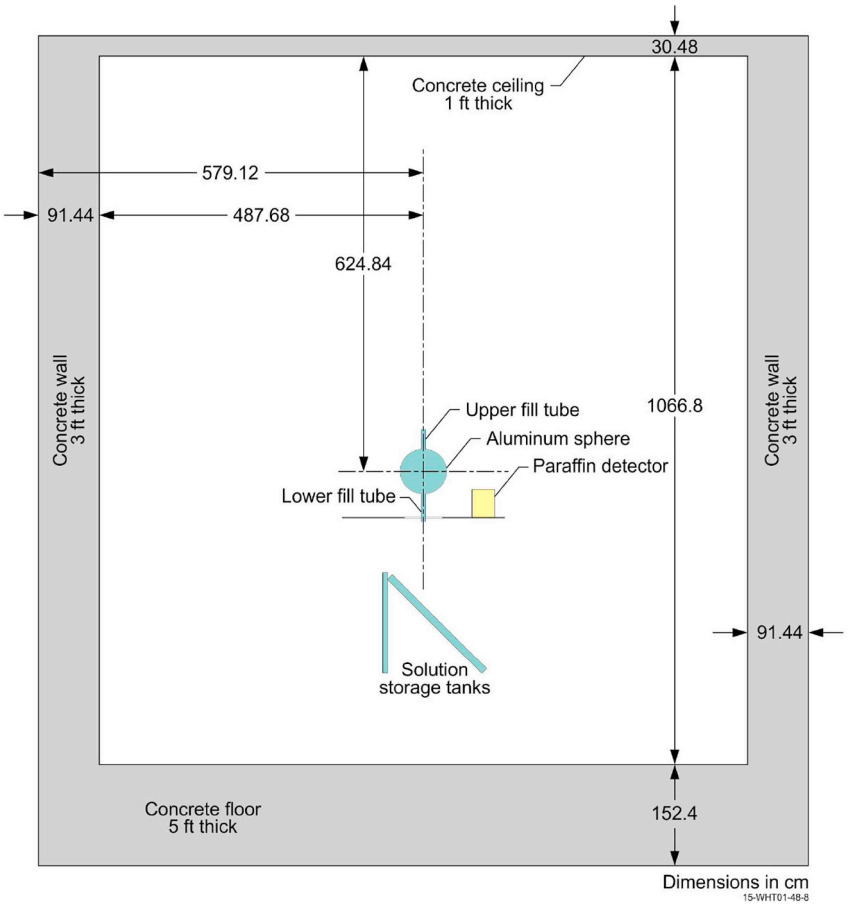

Fig. 6. View of the detailed computational model used for the evaluation of bias due to the surrounding structure.

Table 4
Biases in k_{eff} due to simplifications in the benchmark model for the criticality evaluation.

Bias	Δkeff ± σ_{calc}
Air removal	Neg. ± 0.00009
Al type	0.00015 ± 0.00009
heresite	−0.00057 ± 0.00009
Surrounding structure	−0.00057 ± 0.00029
Solution impurities	0.00443 ± 0.00013
Departure from sphericity	0.00019 ± 0.00009
Total simplification bias	**0.00363**± 0.00037

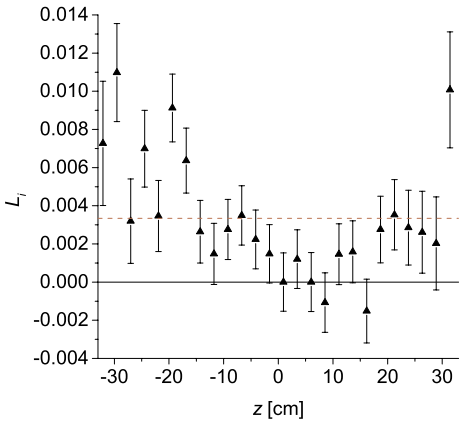

Fig. 7. Bias of the reaction rate distribution calculated with the detailed model represented with L_i values as a function of radial distance from the center of the sphere (radial positions in calculations are equal to the experimental positions of moving detector). Dashed red line represents average value of L_i through the entire radial profile.

Table 5
Calculated k_{eff} of the benchmark model for the criticality experiment.

	k_{eff}	σ_{calc}	(C-E)[a]	(C-E)/E[a]	(C-E)/σ_E
MCNP 6.1.0	0.99940	± 0.00006	−0.00470	−0.5%	−0.72
COG 11.1	0.99943	± 0.00013	−0.00467	−0.5%	−0.72
KENO V.a	0.99843	± 0.00008	−0.00567	−0.6%	−0.87

[a] 'C' is the calculated value and 'E' is the expected or benchmark value.

The overall bias contribution for the reaction rate evaluation was calculated using reaction rate benchmark model (see Fig. 4), where the following simplifications were made and structures were removed: air surrounding the sphere, remaining surrounding structures (paraffin detectors, storage tanks, supporting legs), room (walls, floor and ceiling - see Fig. 6), aluminium impurities, and solution impurities. Similar to the evaluation of uncertainties, the biases were also evaluated through the entire radial profile. When evaluating the bias contribution it is important to know the sign of the change, therefore instead of evaluating the L_{rs} values the L_i values were used and each measuring position was treated individually. The negligible limit of $L_i < 0.001$ was chosen. Bias results are presented in Fig. 7.

5.2. Benchmark values

The k_{eff} bias value of the benchmark model given in Table 4 was added to the experimental k_{eff} of 1.0005 to obtain the benchmark model $k_{eff} = 1.0041 \pm 0.0065$, taking into account that the uncertainty is equal to the sum of the squares of experimental and bias uncertainty. The k_{eff} values calculated using the MCNP 6.1.0, COG 11.1 (Buck and Lent, 2002) and KENO V.a (SCALE 6.1 (Rearden and Jessee, 2016)) Monte Carlo transport codes with ENDF/B-VII.1 (Chadwick et al., 2011) cross sections for benchmark model are summarized in Table 5.

Table 6
MCNP 6.1.0 sample calculation results for the criticality benchmark using different nuclear data libraries.

	k_{eff}	σ_{calc}	(C-E)[a]	(C-E)/E[a]	(C-E)/σ_E
ENDF/B-VII.1	0.99940	± 0.00006	−0.00470	−0.5%	−0.72
JEFF 3.3	0.99878	± 0.00006	−0.00532	−0.5%	−0.82
JENDL 4.0	1.00059	± 0.00006	−0.00351	−0.3%	−0.54

[a] 'C' is the calculated value and 'E' is the expected or benchmark value.

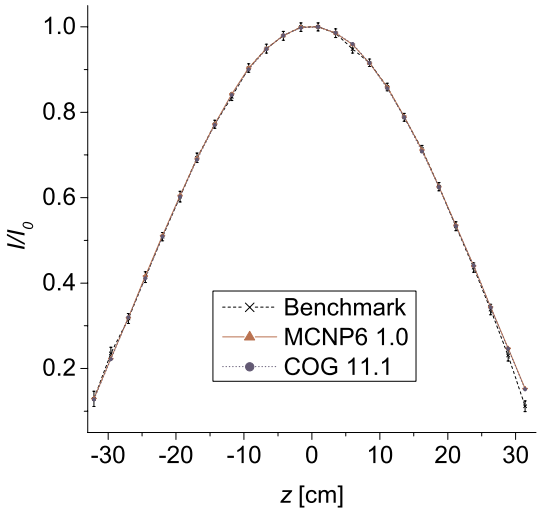

Fig. 8. Normalized fission rate radial profile calculated with MCNP 6.1.0 (red) and COG 11.1 (blue) compared to evaluated simplified benchmark value (black) as a function of radial distance from the center of the sphere (radial positions in calculations are equal to the experimental positions of moving detector).F

They were compared to the benchmark model k_{eff}. It can be concluded that results using different Monte Carlo codes agree well with each other and deviate from the experimental value by ~500 pcm, which is within the experimental uncertainty. Results obtained with MCNP using different nuclear data libraries are provided in Table 6, where it can be observed that different nuclear data libraries deviate by ~180 pcm between each other and are all within the experimental uncertainty.

After evaluating experimental uncertainty and bias contributions, the benchmark fission rate radial profiles were calculated and are presented in Fig. 8. There is good agreement between different codes and the benchmark values with deviations within the uncertainties. For a better view of deviations the $(C/E) - 1$ and $(C - E)/\sigma$ graphs are presented in Fig. 9, where C stands for calculated value and E is the benchmark model value. The only outlying position is the last position at the top of the sphere, where the deviation is greater than 3σ. The reason for the deviation is believed to be the scarce information on the surrounding structures.

6. Cross section sensitivity and uncertainty analyses of k_{eff}

Two codes which use two different methods for nuclear data uncertainty determination were used for the analysis. The results of the two different approaches to nuclear data uncertainty propagation through the neutron transport simulation are presented at the end of this section.

The first method is a well known and validated 3D nuclear data sensitivity and uncertainty code SUSD3D (Kodeli, 2001) which utilizes

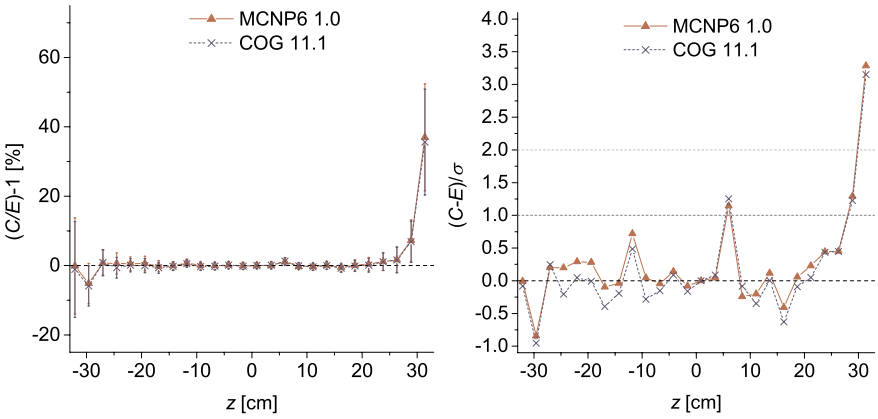

Fig. 9. Deviations between benchmark value (E) and the calculated value (C) using MCNP 6.1.0 (red) and COG 11.1 (blue) for the reaction rate evaluation as a function of radial distance from the center of the sphere (radial positions in calculations are equal to the experimental positions of moving detector). The connecting lines serve as an eye-guide only. The black dashed line represents zero (complete agreement between both values). On the right hand-side graph grey dashed lines represent 1σ and 2σ values.

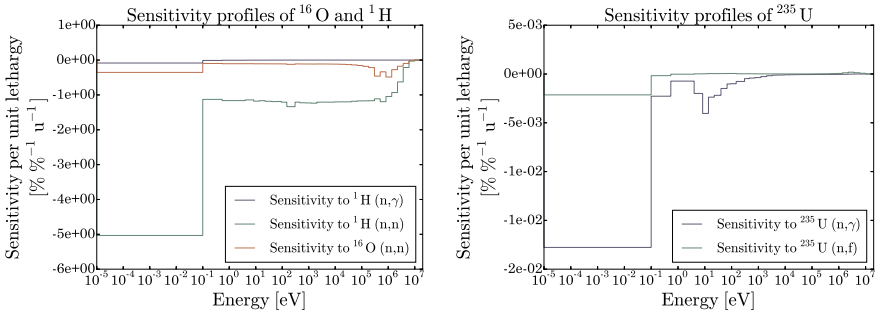

Fig. 10. Sensitivity profiles calculated with SUSD3D for the major contributors to the uncertainty: the elastic scattering cross section (n,n) of ^{16}O, the capture cross section (n,γ) and the elastic scattering cross section (n,n) of ^{1}H (left), the capture cross section (n,γ), the fission cross section (n,f) of ^{235}U (right). One can observe, that the sensitivities are higher in the thermal energy region.

the first order discrete ordinates formulation of perturbation theory to determine the relative nuclear data sensitivity profiles. The sensitivity profiles are folded with the appropriate nuclear data covariance matrices to obtain the desired relative uncertainties.

The SANDY (Fiorito et al., 2016) (SAmpler of Nuclear Data and uncertaintY) code is based on the basic theory of stochastic (Monte Carlo) sampling to propagate nuclear data covariance information through the neutron transport model under study. In the first step SANDY retrieves nuclear data parameter best estimates and covariance matrices (when available) from the nuclear data files in the ENDF-6 format (CSEWG, 2013). Then the nuclear data are sampled into random sets according to the chosen multivariate probability density function (PDF) for the uncertain variables, i.e. normal or lognormal. The process ensures that the random samples are distributed in the input phase space according to the original covariance matrix. In the final step the random nuclear data samples are written back into perturbed ENDF-6 format files. The perturbed files are then used in a series of simulations using a preferred transport solver. Statistical tests are performed on the results in order to determine the uncertainty due to the perturbed nuclear data.

In order to determine the sensitivity profiles and uncertainties using SUSD3D, first the forward and adjoint transport calculations for the IEU-SOL-THERM-005 criticality benchmark were performed with the PARTISN (Alcouffe et al., 2008) discrete ordinates deterministic transport solver. The computational model was based on the MCNP simplified benchmark model. The nuclear data was taken from the ENDF/B-VII.1 evaluation and was processed into 33 energy groups. The SUSD3D code was used next to perform the nuclear data sensitivity and uncertainty analysis. The sensitivity of the calculated k_{eff} with respect to the variation of partial reaction cross sections of ^{1}H, ^{16}O, ^{27}Al, ^{234}U, ^{235}U, ^{236}U and ^{238}U were studied. Due to the lack of processed multigroup nuclear data of ^{19}F for PARTISN, the ^{19}F partial reaction cross sections uncertainties were only calculated with SANDY and found to be negligible. In addition to the forward and adjoint flux moments, SUSD3D requires nuclear data covariance matrices in order to determine the nuclear data uncertainties. Covariances were taken from the JEFF-3.3, JENDL-4.0u, SCALE-6.0m and ENDF/B-VII.1 libraries and processed with the ANGELO (Kodeli et al., 2010) and/or NJOY (MacFarlane et al., 2012) codes into the appropriate 33-group structure and format. The sensitivity/uncertainty calculations with SUSD3D were performed using the XSUN-2017 (Kodeli and Slavic, 2017) suite which is a Windows based graphical user interface combining the TRANSX (MacFarlane, 1992), PARTISN, and SUSD3D codes into a single sequential user friendly work-flow. The above mentioned 33-group cross sections and covariance matrices are also included in the XSUN-2017 package (Kodeli and Slavic, 2017).

Based on the SUSD3D results the five reactions which contribute to the largest uncertainty were identified. These are the capture cross section (n,γ), the fission cross section (n,f) of ^{235}U, the elastic scattering cross section (n,n) of ^{16}O, the capture cross section (n,γ) and the elastic scattering cross section (n,n) of ^{1}H.[3] The sensitivity profiles calculated with SUSD3D for these five reactions are shown in Fig. 10.

In the first step of the second method used to determine nuclear data uncertainty, randomly sampled cross sections for these five reactions were generated with the SANDY code. All the perturbed ENDF-6 format files were processed into ACE format using NJOY (MacFarlane et al., 2012), and a series of criticality calculations was performed with each of the perturbed files with MCNP 6.1.0. The statistical uncertainty of each MCNP k_{eff} calculation was 25 pcm. In the second step the remaining cross sections, which according to SUSD3D results negligibly contributed to the uncertainty due to nuclear data, were analysed. The remaining cross sections uncertainties are about 30 pcm which is of the order of magnitude of the statistical uncertainty of individual k_{eff} calculated by MCNP and therefore negligible as predicted by SUSD3D.

The results of the statistical analysis of the simulation results with SANDY produced perturbed cross sections are given in Fig. 11. The k_{eff} results in the figure are sorted to 50 bins, a normal distribution (red dashed line) is fitted to the results and the mean (μ) and standard

[3] At the time of writing of this article SANDY cannot process covariances of the average fission neutron multiplicity ($\bar{\nu}$).

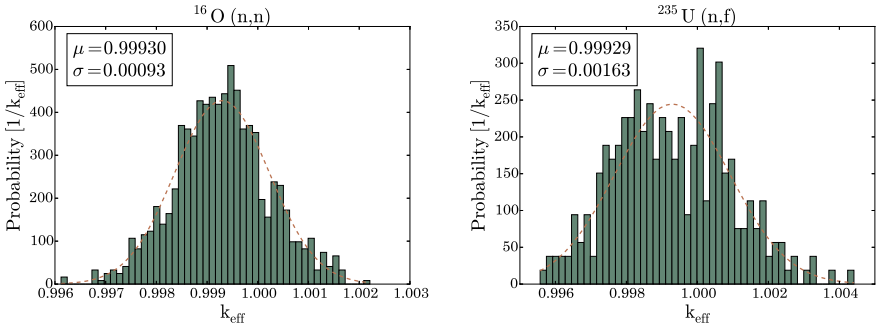

Fig. 11. Statistical analysis of the k_{eff} results with perturbed cross sections produced by SANDY. Results (mean value μ and standard deviation σ) of the propagation of uncertainties of two different cross sections (elastic scattering cross section (n,n) of ^{16}O and the fission cross section (n,f) of ^{235}U) through the neutron transport simulation are given. The ENDF/B-VII.1 library was used for the analysis.

Table 7
Benchmark k_{eff} sensitivities to nuclear data and uncertainties due to nuclear data uncertainties calculated with the JEFF-3.3, JENDL-4.0, SCALE-6.0 and ENDF/B-VII.1 covariance libraries and two different codes - SUSD3D and SANDY. The MT numbers refer to the nomenclature of the ENDF-6 format (CSEWG, 2013).

Nuclide	Reaction\MT number	Sensitivity [%/%]	SUSD3D [pcm]				SANDY [pcm]
			JEFF- 3.3	JENDL- 4.0	SCALE- 6.0	ENDF/B- VII.1	ENDF/B- VII.1
	(n,n)\2	$3.09\cdot10^{-1}$	270.1	NP[a]	233.9	NP	250
	(n,γ)\102	$-3.71\cdot10^{-1}$	947.4	NP	185.5	NP	1024
^{16}O	(n,n)\2	$6.21\cdot10^{-2}$	109.1	88.0	75.7	109.8	93
	(n,n')\4	$6.87\cdot10^{-4}$	12.5 [b]	4.7	7.1	8.1	32[c]
^{19}F	(n,n')\4	NC[d]	NC	NC	NC	NC	32
	(n,γ)\102	NC	NC	NC	NC	NC	31
^{235}U	(n,n')\4	$1.15\cdot10^{-4}$	0.6	1.2	0.7	0.7	29
	(n,f)\18	$5.34\cdot10^{-1}$	346.9	188.4	203.0	188.7	180
	(n,γ)\102	$-8.14\cdot10^{-2}$	114.7	127.6	150.0	127.7	138
	$\bar{\nu}$\452	$9.99\cdot10^{-1}$	561.1	307.8	307.5	705.4/138.4[e]	NC
	(n,n)\2	$2.87\cdot10^{-4}$	0.2	0.3	0.7	0.6	32
	(n,n')\4	$2.52\cdot10^{-4}$	1.6	2.2	4.4	4.5	33
	(n,f)\18	$4.50\cdot10^{-4}$	1.3	0.3	0.2	0.2	32
	(n,γ)\102	$-1.72\cdot10^{-2}$	19.4	26.0	21.4	26.0	35
	$\bar{\nu}$\452	$6.25\cdot10^{-4}$	0.6	0.4	0.7	0.7	NC
Total			1210	419	525	762\320[6]	NC

[a] Covariance not processed (NP).
[b] An error of a factor of 100 in the JEFF-3.3 ^{16}O inelastic covariance matrix was corrected.
[c] In the order of the MCNP statistical uncertainty (25 pcm).
[d] Not calculated (NC).
[e] Using total $\bar{\nu}_t$\prompt $\bar{\nu}_p$ covariances.

deviation (σ) are given. The results of k_{eff} from 1000 perturbed elastic scattering cross section (n,n) of ^{16}O samples were analysed in Fig. 11 (left) and 300 perturbed fission cross section (n,f) of ^{235}U samples were analysed in Fig. 11 (right). 300 random samples per cross section were found to be sufficient in order to show that normal distribution of the results is achieved. Codes based on random sampling such as SANDY require large amounts of CPU time but can, in principal, be used with any transport solver. For now SANDY is limited to the ENDF-6 format for its input and output data.

The results of the SUSD3D sensitivity and uncertainty analysis and the SANDY uncertainty analysis are given in Table 7. The sensitivities calculated by SUSD3D of the calculated k_{eff} with respect to the most important nuclear data are listed in the third column. The sensitivities are integrated over the whole energy range and are given in terms of the percentage of change in k_{eff} per 1% change of the cross section for a given nuclide (first column) and reaction type (second column).

k_{eff} was found to be very sensitive to the average fission neutron multiplicity ($\bar{\nu}$), fission cross section (n,f) and capture cross section (n,γ) of ^{235}U, capture cross section (n,γ) and elastic scattering cross section (n,n) of ^{1}H, and the elastic scattering cross section (n,n) of ^{16}O. The inelastic scattering cross section (n,n') sensitivities for all nuclei are negligible. Note that, for example, a negative sensitivity (as defined in equation (1)) of 0.37%/% means that k_{eff} is reduced by 0.37% (370 pcm) if the ^{1}H capture cross section (n,γ) in the whole energy range is increased by 1%. The corresponding uncertainties calculated with SUSD3D using the JEFF-3.3, JENDL-4.0u, SCALE-6.0m, and ENDF/B-VII.1 covariance data are listed in columns 4–7, respectively. The uncertainties calculated with SANDY and using ENDF/B-VII.1 cross sections and covariance data are given in column 8.

As noted above the largest uncertainties are due to the uncertainties in the capture cross section (n,γ), the fission cross section (n,f) and the average fission neutron multiplicity ($\bar{\nu}$) of ^{235}U and the uncertainties in the elastic scattering cross section (n,n) and capture cross section (n,γ) of ^{1}H. This result is to be expected when taking into consideration the highly thermalized spectrum of the experiment shown on the left side of Fig. 12. The negligible uncertainty due to ^{19}F can also be explained by considering the spectrum and total cross section of ^{19}F shown in Fig. 12.

The uncertainties in the capture cross section of ^{235}U agree among all of the covariance libraries, however the uncertainties in $\bar{\nu}$ and fission cross section differ considerably. An inconsistency between the total ($\bar{\nu}_t$) and the prompt ($\bar{\nu}_p$) average fission neutron multiplicity covariance matrices of ^{235}U in the ENDF/B-VII.1 evaluation can be observed, suggesting a probable underestimation of the ($\bar{\nu}_p$) covariances. This was corrected in the recent ENDF/B-VIII evaluation. Another interesting cross section is the elastic scattering cross section (n,n) of ^{16}O which contributes an uncertainty between 88 pcm and 110 pcm when using the different covariance libraries. According to the SCALE-6.0 and JEFF-3.3 covariance libraries, hydrogen cross section uncertainties are

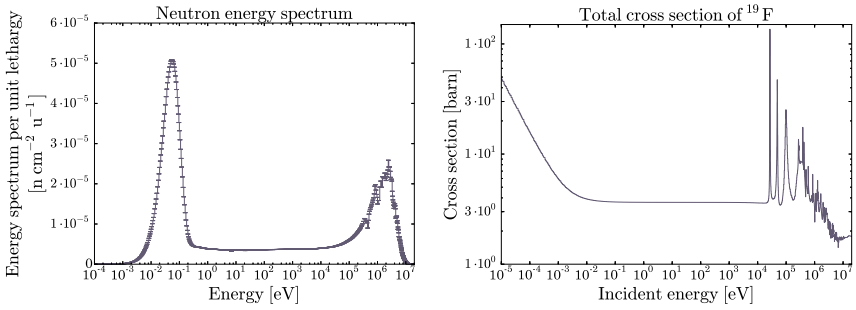

Fig. 12. Neutron lethargy spectra calculated in the 640 SAND-II energy group structure with the ENDF/B-VII.1 nuclear data library for the reference eigenvalue case (left) and the total neutron cross section taken from ENDF/B-VII.1 for ^{19}F (right).

of the same order of magnitude as the uncertainties in ^{235}U. In the case of the JEFF-3.3 library the capture cross section (n,γ) on hydrogen is the largest contributor to the total uncertainty given in the last row.

SANDY is a newly developed code and has not yet been validated thoroughly. The agreement between the widely validated SUSD3D code and SANDY is satisfactory. Excellent agreement between the results of the codes for the capture cross section (n,γ) and the fission cross section (n,f) of ^{235}U, the elastic scattering cross section (n,n) of ^{16}O and the elastic scattering cross section (n,n) of ^{1}H can be observed.

7. Conclusions

A complete evaluation of experimental and computational nuclear data uncertainties for the criticality and fission rate radial profile experiments performed in 69.2 cm diameter sphere containing intermediate enriched UO_2F_2 solution is presented. A detailed description of the experiments and evaluation of experimental uncertainty can be found in the ICSBEP (IEU-SOL-THERM-005) and IRPhEP (ORCEF-FUND-EXP-001) Handbooks. It was found that the largest contribution the uncertainty in k_{eff} was due to the uncertainty in the uranium enrichment (~550 pcm) and the largest contributions to the uncertainty in the radial fission rate profile was due to the uncertainty in the moving detector guide tube diameter and moving detector radial position. It was also found that the experiment is highly sensitive to the H-H_2O thermal scattering kernel and can therefore be used to validate different nuclear data libraries and methods for generating the thermal scattering kernel at the desired temperature. ENDF/B-VII.0 and JEFF 3.1 thermal scattering kernels were compared and deviations up to 100 pcm were observed. When comparing different methods it was found that the results obtained with the LEAPR module of the NJOY code and the results obtained with MAKXSF code or using mixing method agree well with each other and the deviations are <100 pcm. After analysing the experimental uncertainties and bias value, benchmark value of k_{eff} was calculated using different Monte Carlo codes and the results deviate from the experimental value by ~500 pcm, which is within the experimental uncertainty. Benchmark values of radial fission rate distribution were calculated using two Monte Carlo codes and their results are in agreement with the deviations within the uncertainties. Calculated results also agree well with the experiments, with the only exception being the last position at the top of the sphere, where the deviation is greater then 3σ. It is assumed that the reason for this deviation is scarce information regarding the surrounding structures. In MCNP it is assumed that different parameters are uncorrelated, which may not be true, especially in case of reaction rate values in measuring positions lying close to each other. The correlation between different parameters from a single Monte Carlo calculation will be studied in future research.

In this paper the evaluation of experimental uncertainties was supplemented by the evaluation of uncertainties in nuclear data. The total uncertainties calculated using four different covariance libraries (JEFF-3.3, JENDL-4.0, SCALE-6.0 and ENDF/B-VII.1) were 1210 pcm, 419 pcm, 525 pcm and 762 pcm, respectively. The largest contributors to the uncertainty are the capture cross section, the fission cross section and the average fission neutron multiplicity of ^{235}U, the elastic scattering cross section of ^{16}O and the capture cross section and elastic scattering cross section of ^{1}H which all have large sensitivities in the thermal energy region. Two fundamentally different methods for neutron cross section uncertainty analysis were used and compared. The results between the SUSD3D and SANDY codes agree very well. It is also planned to validate SANDY on a series of simple criticality benchmarks.

Acknowledgements

The authors would like to acknowledge the work done by Michelle Pitts and Farzad Rahnema who have evaluated a similar series of experiments in the same spherical tank indexed as HEU-SOL-THERM-013 (ICSBEP, 2016). Their gathered information and results were of great help in our evaluation and invaluable to the quality of the benchmark evaluation. Authors would like to express gratitude for the comprehensive review and support provided by the ICSBEP and IRPhEP technical review group.

The authors acknowledge the financial support from the Slovenian Research Agency (research core funding No. P2-0073 and project for training young researchers No. 1000-15-0106). The authors would also like to acknowledge the Memorandum of Understanding between SCK·CEN and JSI project agreement CO-90-16-4272-01.

References

Alcouffe, R.E., Baker, R.S., Dahl, J.A., Turner, S.A., Ward, R., 2008. PARTISN: a Time-dependent, Parallel Neutral Particle Transport Code System. LA-UR-08-07258. (Revised Nov. 2008).

Briggs, J.B., Bess, J.D., June 2011. Development of an ICSBEP Benchmark Evaluation, Nearly 20 Years of Experience, vol 2011 American Nuclear Society Annual Meeting, INL/CON-10-20745.

Briggs, J.B., Bess, J.D., Gulliford, J., 2014. Integral benchmark data for nuclear data testing through the ICSBEP & IRPhEP. Nucl. Data Sheets 118, 396–400.

Brown, F.B., 2006. The Makxsf Code with Doppler Broadening. LA-UR-06-7002.

Buck, R.M., Lent, E.M., 2002. COG User's Manual: a Multiparticle Monte Carlo Transport Code, fifth ed. Lawrance Livermore National Laboratora, Livermore CA UCRL-TM-202590.

Callihan, D., February 7, 1975. Critical Dimensions of Aqueous Solutions of U(37)O2F2. Y-DR-135, Oak Ridge Y-12 Plant.

Chadwick, M.B., et al., Dec 2011. ENDF/B-VII.1 nuclear data for science and technology: cross sections, covariances, fission product yields and decay data", LA-UR 11-05121, los alamos national laboratory, also. Nucl. Data Sheets 112 (12), 2887–2996.

Chadwick, M.B., et al., 2006. ENDF/B-VII.0: next generation evaluated nuclear data library for nuclear science and technology. Nucl. Data Sheets 107 (12), 2931–3060.

Conlin, J.L., Ji, W., Lee, J.C., Martin, M.R., 2005. Pseudo material construct for coupled neutronic-thermal-hydraulic analysis of VHTGR. Trans. ANS 91.

CSEWG, 2013. ENDF-6 Formats Manual. Data Formats and Procedures for the Evaluated Nuclear Data Files ENDF/B-VI and ENDF/B-VII. Upton, USA.

Dean, V.A., 2003. The benchmark evaluation process: from experimental data to benchmark model. Nucl. Sci. Eng. 145, 20–38.

Donnelley, J.V., 2010. Interpolation of temperature-dependent nuclide data in MCNP. Nucl. Sci. Eng. 168, 180–184.

Elam, K.R., 2016. Water reflected ^{233}U uranyl nitrate solutions in simple geometry, U233-

SOL-THERM-005. In: International Handbook of Evaluated Criticality Safety Benchmark Experiments [DVD]/Nuclear Energy Agency. OECD Nuclear Energy Agency, Paris, pp. 37.
Fiorito, L., Žerovnik, G., Stankovskiy, A., Van den Eynde, G., Labeau, P.E., 2016. Nuclear data uncertainty propagation to integral responses using SANDY. Ann. Nucl. Energy 101, 359–366.
Goorley, T., et al., Dec 2012. LA-UR-11-07082. Initial MCNP 6 Release Overview, vol 180. Los Alamos National Laboratory, also Nuclear Technology, pp. 298–315.
Goričanec, T., Žerovnik, G., Snoj, L., 2018. Radial fission rate profiles in aqueous solution of U(37 %)O_2F_2 in spherical geometry. ORCEF-FUND-EXP-001 In: International Handbook of Evaluated Reactor Physics Benchmark Experiments [DVD]/Nuclear Energy Agency. OECD Nuclear Energy Agency, Paris, pp. 84.
Gwin, R., Magnuson, D.W., 1960. Critical Experiments for Reactor Physics Studies. CF 60-4-12. Oak Ridge National Laboratory September 16.
International Handbook of Evaluated Criticality Safety Benchmark Experiments. OECD Nuclear Energy Agency, Paris [DVD]/Nuclear Energy Agency.
International Handbook of Evaluated Reactor Physics Benchmark Experiments [DVD]/Nuclear Energy Agency. OECD Nuclear Energy Agency, Paris, pp. 6589 (NEA;7329).
Kaiba, T., Žerovnik, G., Snoj, L., Lengar, I., 2016. Unreflected critical dimension of aqueous solution of U(37 %)O2F2 in spherical geometry. IEU-SOL-THERM-005 In: International Handbook of Evaluated Criticality Safety Benchmark Experiments [DVD]/Nuclear Energy Agency. OECD Nuclear Energy Agency, Paris, pp. 58.
Kodeli, I., 2001. Multidimensional deterministic nuclear data sensitivity and uncertainty code system, method and application. Nucl. Sci. Eng. 138, 45–66.
Kodeli, I., Slavic, S., 2017. SUSD3D computer code as part of the XSUN-2017 Windows interface environment for deterministic radiation transport and cross-section sensitivity-uncertainty analysis. Sci. Technol. Nucl. Install. 2017, 1264736 16. https://doi.org/10.1155/2017/1264736.
Kodeli, I., Sartori, E., Feb 2010. ANGELO-LAMBDA, Covariance Matrix Interpolation and Mathematical Verification. https://www.oecd-nea.org/tools/abstract/detail/nea-1798.
Koning, A., Forrest, R., Kellett, M., Mills, R., Henriksson, H., Rugama, Y., 2006. "The JEFF-3.1 Nuclear Data Library", JEFF Report 21, Nuclear Energy Agency, Orgarnization for Economic Co-operation and Development, NEA No. 6190. OECD.
MacFarlane, R., Muir, D., Boicourt, R., Kahler, A., 2012. The NJOY Nuclear Data Processing System, Version 2012. LANL Tech. Rep. LA-UR-12-27079.
MacFarlane, R.E., July 1992. TRANSX2: a Code for Interfacing MATXS Cross-section Libraries to Nuclear Transport Code. LA-12312-MS.
Magnuson, D.W., November 1973. Critical Concentration of U(37)O_2F_2 Aqueous Solution in an Unreflected 69.2-cm-diameter Aluminum Sphere. Y-DR-118, Oak Ridge Y-12 Plant.
Magnuson, D., 1958. BOOK43R - Notebook ETA. Oak Ridge National Laboratory. https://rsicc.ornl.gov/CriticalExperiments/book43r.pdf, Accessed date: 25 July 2016.
Marshall, M.A., et al., 2010. Water-moderated and -Reflected Slabs of Uranium Oxyfluoride. HEU-SOL-THERM-034, NEA/NSC/DOC/(95)03/II.
Pitts, M., et al., 1996. Unreflected 174-liter Spheres of Enriched Uranium Nitrate Solutions. HEU-SOL-THERM-013 NEA/NSC/DOC/(95)03/II.
Plompen, A., November 2017. Announcing JEFF-3.3 Release. CHANDA/JEFF Meetings, NEA Headquarters, Paris France JEFDOC-1864. https://www.oecd-nea.org/dbdata/nds_ jefdoc/jefdoc-1864.pdf.
Rearden, B.T., Jessee, M.A., 2016. SCALE Code System, ORNL/TM-2005/39, Version 6.2. Oak Ridge National Laboratory, Oak Ridge, Tennessee.
Shibata, K., Iwamoto, O., Nakagawa, T., Iwamoto, N., Ichihara, A., Kunieda, S., Chiba, S., Furutaka, K., Otuka, N., Ohsawa, T., Murata, T., Matsunobu, H., Zukeran, A., Kamada, S., Katakura, J., 2011. JENDL-4.0: a new library for nuclear science and engineering. J. Nucl. Sci. Technol. 48 (1), 1–30.
Snoj, L., Kodeli, I., 2014. Evaluation of the KRITZ-2 criticality and reaction rate benchmark experiments. Nucl. Sci. Eng. 178, 496–508.